RSC Advances

ROYAL SOCIETY OF CHEMISTRY

www.rsc.org/advances

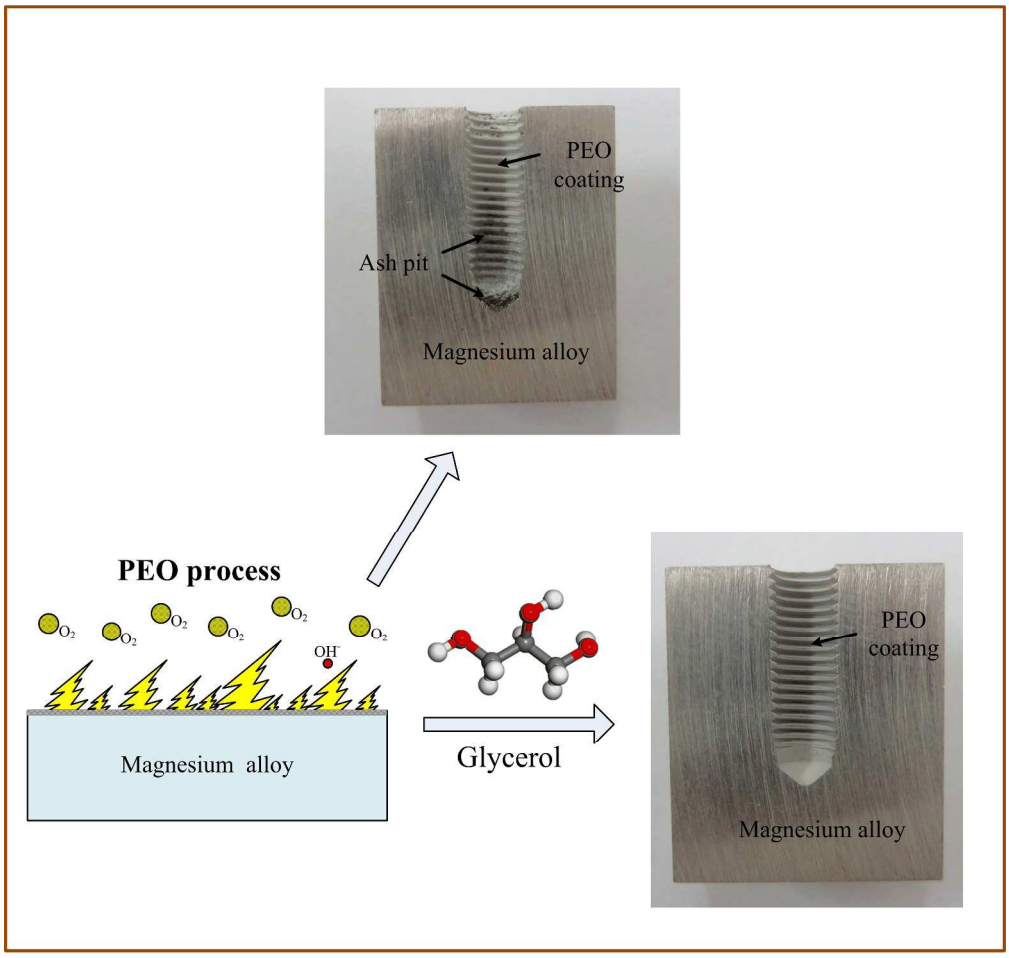

334x316mm (300 x 300 DPI)

Glycerol as a leveler on ZK60 magnesium alloys during the plasma electrolytic oxidation

Zhaozhong Qiu[1], Yushen Zhang[1],Yuemei Li[1], Jinchao Sun[2], Rui Wang[1]*, Xiaohong Wu[1]

(1. Department of Chemistry, Harbin Institute of Technology, Heilongjiang 150001, PR China.

2. Department of Mechanical Engineering, Huaiyin Institute of Technology, Jiangsu 223003, PR China.)

Corresponding author: wangrui001@hit.edu.cn

Tel.: Phone number: +086-15846590861

Xidazhi Street #92, Harbin, Heilongjiang 150001, PR China

Abstract

Glycerol ($C_3H_8O_3$), an organic waste generated by the biodiesel industry, has been recently proposed as a valuable green additive. The influence of glycerol on the morphology, composition and corrosion resistance of ZK60 magnesium alloys during the plasma electrolytic oxidation process has been investigated. The adsorption behavior of $C_3H_8O_3$ molecules on Mg (002) surface has been studied by using molecular dynamics simulations. Results predict that $C_3H_8O_3$ could be used as a promising leveler during the plasma electrolytic oxidation process. The silicate electrolyte with glycerol could increase the unit-area adsorptive capacity of the negative ions at the anode-electrolyte interface, and thus improves the smoothness and corrosion resistance of the coating.

Keywords: Magnesium alloy, Corrosion resistance, Molecular dynamics simulations.

Introduction

ZK60 alloys have been widely applied in the fields of aeronautical engineering, mechanical device, consumer electronics and artificial human bones in the last two decades [1]. The key advantage of ZK60 over other metals is their excellent strength-to-weight ratio [2,3]. Nevertheless, the ZK60 alloys have relatively poor corrosion resistance due to the high reactivity of the magnesium alloy [4-6], which limits its practical applications. Plasma electrolytic oxidation (PEO) is one of the most effective methods to enhance the corrosion and wear resistance of the metals by forming an appropriate thickness and density of coating on the magnesium alloys [7].

PEO coating as a barrier to the environment could inhibit the invasion of corrosive media such as Cl^- to protect the substrate effectively and improve the corrosion resistance of the metal remarkably. And the PEO coating properties are mainly determined by the electrolytes used in the PEO process. At present, inorganic electrolytes, such as silicate [8,9], aluminate [10,11], borate [12] and phosphate [13] are often used in environmentally friendly processes in PEO treatment. However, organic substances are seldom applied [14-16].

Glycerol ($C_3H_8O_3$) has three hydroxyl groups that are responsible for its high solubility in water and its hygroscopic nature [17]. Similar with other polar solvents such as water, DMSO and DMF, glycerol is able to facilitate dissolution of inorganic salts [18]. Crucially, this organic additive is not toxic [19]. The presence of glycerol as an additive in the plating bath could modify the current density to affect the morphology of the deposits [20]. The influence of the polyalcohol sorbitol or glycerol on the electrodeposition of other metals or alloys [21,22] been widely studied. For example, Morachevskii et al [23] used alkaline glycerol solutions to separate the active substance from battery plate grids. It was widely accepted [20-22, 24] that

glycerol could hinder the passivation of the anode and dissolve the oxide fraction of the scrap. Therefore, glycerol would be an intriguing choice which used as a promising leveler during the PEO process.

In this context, it would be invaluable to find out what influence glycerol has on the PEO process of deposition. The effects of glycerol on morphological characteristics and corrosion protection of the coatings were also investigated. The absorption of glycerol could change the solid-liquid interface compositions and affect the area of spark discharge to avoid the partial sintering during the PEO process. And glycerol may be used as a leveler for close-hole during the plasma electrolytic oxidation process. Therefore, MD simulation was used for discussing the interaction between $C_3H_8O_3$ and ZK60 magnesium alloy surface.

2. Experimental Procedures

2.1. Preparation of PEO coatings

Rectangular coupons (25 mm×20 mm×5 mm) of ZK60 Magnesium alloy (mass fraction: Zn 5wt.%, Zr 0.3 wt.%, Mn 0.1 wt.% and balance Mg) were used as the substrate material in this study. They were abraded successively with 180, 600, 1000 and 2000 grit emery sheets and cleaned with acetone before the PEO treatment. Homemade pulsed bipolar electrical source with a power of 5 kW was used for PEO in a water-cooled electrobath made of stainless steel, which also served as the counter electrode. The reaction temperature of the electrolytes during the processing was kept at 20±5 °C by adjusting the cooling water flow. PEO process equipment was similar to the one presented by Matthews' group[25]. An aqueous electrolyte was prepared from a solution of Sodium silicate (20 g/L), potassium hydroxide (7 g/L) and sodium fluoride (1 g/L). The electronic power frequency was fixed at 1000 Hz. The duty ratios of two pulses were both equal to 10%. The applied current density was 0.6

A/dm^2. After PEO treatment, the coated samples were rinsed with deionized water and dried in the air.

2.2. Molecular dynamics simulations

Molecular dynamic (MD) simulations of the interaction between $C_3H_8O_3$ and the magnesium surface were carried out in a simulation box (3.209 nm×3.209 nm× 4.138 nm) with periodic boundary conditions using Materials Studio (from Accelrys Inc). The box consists of a magnesium surface, a liquid phase and a vacuum layer of 1 nm height. The Mg crystal was cleaved along the (002) plane because of the maximum of peak intensity. The liquid phase contained water molecules with a density of 1 g/cm^3 and five $C_3H_8O_3$ molecules. The MD simulations were performed at 298 K, NVT ensemble with a time step of 1 fs and simulation time of 2 ns in water solution. The MD simulations were performed with the discover program. For the whole simulation procedure, the forcefield CVFF was used[26]. The CVFF (consistent-valence forcefield) was a generalized valence forcefield fitted to small organic, such as amides, carboxylic acids, etc., and metal crystal. It was primarily intended for studies of structures and bind energies, and it also predicted vibrational frequencies and conformational energy reasonably well.

The interaction energy $E_{\text{Mg-C}_3\text{H}_8\text{O}_3}$ between the magnesium surface and $C_3H_8O_3$ was calculated as [27]:

$$E_{\text{Mg-C}_3\text{H}_8\text{O}_3} = E_{\text{complex}} - E_{\text{Mg}} - E_{\text{C}_3\text{H}_8\text{O}_3} \quad (1)$$

Where E_{complex} stands for the total energy of the magnesium crystal together with the adsorbed $C_3H_8O_3$, E_{Mg} and $E_{\text{C}_3\text{H}_8\text{O}_3}$ are the total energy of the magnesium crystal and free $C_3H_8O_3$, respectively. The binding energy was the negative value of the interaction energy, $E_{\text{binding}} = -E_{\text{Mg-C}_3\text{H}_8\text{O}_3}$.

2.3. Analysis of composition and structure of PEO coatings

The phase composition of the coating was investigated by X-ray diffraction (XRD), using a Cu Kα source. The surface morphology of the prepared coating was observed using scanning electron microscopy (SEM; Hitachi, SU8010) equipped with energy dispersive spectrometer (EDS). Potentiodynamic polarization experiments were performed through Princeton-4000 electrochemical analyzer. Potentiodynamic polarization curves were used to analyze the corrosive nature of the coatings prepared under different oxidation time during immersion in 3.5 wt.% NaCl solution. Each sample was mounted by paraffin with 1 cm^2 surface exposed. The corrosion potential and the corrosion current density were obtained through the linear analysis of Tafel approximation. All electrochemical measurements were performed with a conventional three electrode system of coated samples as working electrode, a platinum plate as auxiliary electrode and Ag/AgCl (sat KCl) as a reference electrode. All experiments were carried out at room temperature.

3. Results and discussion

3.1. Voltage-time response

The galvanostatic dependencies of positive voltage vs. oxidation time during PEO process are shown in Fig.1. During the PEO process, the current density is kept constantly at 0.6 A/cm^2, while the instantaneous variation of voltage is recorded every 10s during the plasma electrolytic oxidation process. According to the differences in the voltage, oxygen evolution and sparking behavior, the whole anodizing process can be divided into four stages [28]. During the first 50 s, namely, stage I, the voltage rises with time evidently, the upward trend is almost a straight line with a slope of 7 V/s. During this stage, there are no sparks and only some tiny oxygen bubbles could be observed on the surface of the sample, which indicates that magnesium alloy matrix

begins to dissolve and a thin passive film is formed on the surface of the alloy. As the reaction process forward, the positive voltage increases rapidly within the first 50 s. Once the voltage exceeds the breakdown voltage (point A in Fig.1), stage Ⅱ starts, oxygen evolution becomes vigorous and many tiny micro-sparks appear with moving around the surface of magnesium alloy.

Insert Figure 1 Here

During the stage Ⅱ, the cell voltage increases continuously with the processing of the PEO. As the reaction process lasting, the orange micro-sparks becomes buzzing and the oxygen evolution becomes more vigorous than that in previous stages [27]. All these phenomena indicate that the PEO process gets into stage Ⅲ. The increase rate of voltage decreases gradually, and the voltage reaches to a stable value. After 260 s, the voltage during PEO process goes up slightly. The micro-sparks become larger and the sound changes from phonic to harsh in the later period of stage Ⅲ. As can be seen from Fig.1, it is rather obvious that the positive voltage effectively increases by adding the glycerol concentration in the electrolyte, which could promote the growth rate of PEO coatings of magnesium alloy under the same current density condition.

3.2 Thickness of PEO coatings

The variation of thickness of ceramic coatings obtained through PEO treatment for 6 min in base electrolyte containing 0, 50, 100 and 200 mL/L glycerol, respectively, is shown in Fig. 2. It is noticed that the thickness of ceramic coatings increases gradually with the increase of concentration of glycerol. The thickness of coating formed in base electrolytic solution without glycerol addition is 13.89 μm. As the concentration of glycerol adding from 50 to 200 mL/L, the thicknesses increase from 16.33 to 19.84 μm. Therefore, the addition of glycerol into the base electrolyte

results in an increase of the value of coatings thickness. In addition, it can be seen that the addition of glycerol could effectively make the whole coatings uniform. The sidewalls of substrate (showed in Fig. 2b-2d) are not flat before oxidation. But the surface of the coating is flat after PEO process prepared in the base electrolyte with glycerol, whereas the surface of the coating (showed in Fig. 2a) is still not flat after oxidation using the bath without containing glycerol. Therefore, the glycerol could be used as a new leveler during the plasma electrolytic oxidation process.

Insert Figure 2 Here

3.3 Chemical composition and microstructure of the coatings

In order to further investigate the surface structure of PEO, energy-dispersive X-ray spectroscopy (EDS) and element mapping characterization analysis were carried out (Fig.3). Chemical element mapping analysis (Fig. 3c–f) shows that the elements including oxygen (O), carbon (C), magnesium (Mg) and silicon (Si) are homogeneously distributed over the surface.

Insert Figure 3 Here

Fig.4 illustrates the XRD patterns of PEO ceramic coatings processed for 6 min in base electrolyte without and with glycerol addition. It is apparent that PEO coating is mainly constituted with Mg, MgO and Mg_2SiO_4. In the initial stage, the voltage increased evidently with time, there are no spark, but only some tiny oxygen bubbles (reaction 2) appeared on the sample surface (anode), which indicates that the magnesium alloy substrate begins to dissolve (reaction 3) and forms a thin passive film on the surface.

$$4OH^- \rightarrow 2H_2O+O_2+4e^- \quad (2)$$

$$Mg \rightarrow Mg^{2+}+2e^- \quad (3)$$

Insert Figure 4 Here

With the effects of anodic voltage, an anionic coacervate is formed in the magnesium/electrolyte solution boundary. The thickness of coacervate rises with the increase of the voltage. When enough magnesium ions accumulate at the magnesium/electrolyte interfaces, the magnesium ions would combine with SiO_3^{2-} and OH^- to form $Mg(OH)_2$ and Mg_2SiO_4 in the coacervate solution. The interface reaction can be described as,

$$Mg^{2+} + 2OH^- \rightarrow Mg(OH)_2 \quad (4)$$

$$2Mg^{2+} + SiO_3^{2-} + 2OH^- \rightarrow Mg_2SiO_4 + H_2O \quad (5)$$

$$Mg(OH)_2 \rightarrow MgO + H_2O \quad (6)$$

Sharma [29] et al. reported that the dehydration reaction is thermodynamically endothermic. Because the instantaneous temperature in a micro-area is higher than 1000 ^oC [30], $Mg(OH)_2$ in the oxide film could be decomposed into MgO and H_2O [31]. Therefore, Mg_2SiO_4 and MgO deposits on the interface, resulting in the growth of the coating.

3.4 Surface morphologies of PEO coatings

Insert Figure 5 Here

Fig.5 displays the surface morphologies of the PEO coating obtained under containing different concentrations of glycerol. The PEO coatings exhibited the rough and porous microstructure, regardless of the coatings prepared in electrolyte of different glycerol concentrations. Numerous pores with different shapes and some cracks distributed throughout the surface are observed in Fig.5a. The addition of glycerol leads to an obvious change in the surface morphology of ceramic coatings. In other words, ceramic coatings obtained in base electrolyte with glycerol (Fig. 5b–d) have fewer cracks than that obtained in the base electrolytic solution. In particular, as

for the coating formed in the base electrolyte containing 100 mL/L glycerol exhibits the micro-pores with the least micro-cracks in this work.

The breakdown voltage has a logarithmic linear correlation with the thickness of the coatings [32]. The voltage is increased by adding the concentrations of glycerol. The high voltage leads to an enhanced thickness of the coating and increased single pulse energy. The energy of a single pulse is determined by the breakdown voltage (V), peak currents (I) and pulse width (t) (reaction 7).

$$E = \int_0^t V(t)I(t)dt \tag{7}$$

Where E is the energy of single pulse, J; $I(t)$ is the current, A; $V(t)$ is voltage, V; and t is the time, s. The latter resulted in the enlarged pore sizes after the discharged channels are cooled. As the discharge intensity is increasing continuously, accumulated oxide is increased which induces the enlargement of grain size gradually and overlaps of the pores nearby. Therefore the average diameter of the pores is increased significantly, which are due to discharge energy through the channels during the PEO process [33]. It should be noted that the micro-cracks on the surface could be due to thermal stress from the rapid solidification of molten oxide triggering by the electrolyte as a coolant. Moreover, the lower Pilling-Bedworth ratio (PBR) of magnesia (PBR is the ratio of the volume of the elementary cell of a metal oxide to the volume of the elementary cell of the corresponding metal) is also a main reason for the damage of PEO coatings on the magnesium alloys [34].

Insert Figure 6 Here

Fig.6. shows photographs of embedded parts of magnesium alloy after PEO process based in the electrolyte with and without glycerol. It is obvious that there are some ash pits on the surface of PEO coating without glycerol in the electrolyte. The

distribution of the electrical field of thread is uneven during the PEO process, and it is easier to appear the partial sintering in base electrolyte. Compared with the coating prepared in the glycerol electrolyte, the coating is uniform and smooth.

3.5. Molecular dynamics simulations

In order to explain the mechanism of the leveler, molecular dynamics simulations are performed to study the interaction of the organic molecule with metal surfaces [35]. Results obtained from those studies indicate that molecular dynamics simulations can provide insights into the position of the organic molecule systems, and the interaction energy between the organic molecule and metal surface given by molecular dynamics simulations can interpret the adsorption capacity between organic molecule and metal. In order to understand the adsorption mechanism of interaction of $C_3H_8O_3$, MD simulations are performed to study the adsorption behaviors of $C_3H_8O_3$ on the Mg (002) surface. Fig.7(a) shows the initial configuration of the MD simulation boxes. Fig.7(b) is the final equilibrium configuration of the MD simulation boxes. There are only five $C_3H_8O_3$ molecules in our simulation system. The $E_{binding}$ calculated from Fig. 7b is 927.22 kJ/mol. The bigger value of binding energy is easier to adsorb on the surface[26]. Compared with Fig.7(a) and Fig.7(b), the distance between the $C_3H_8O_3$ molecules and Mg surface is decreased. It indicates that $C_3H_8O_3$ could adsorb on the magnesium surface strongly. According to the equilibrium configuration of $C_3H_8O_3$ the adsorbed on Mg (002) surface, we can draw a conclusion that the hydroxyl can be absorbed on the Mg surface. Consequently, the exposed part of Mg surface can be reduced by the covering of $C_3H_8O_3$ molecules, preventing water molecules from contacting with the surface. Furthermore, as the organic molecules could increase the surface resistance and decrease the surface of active sites during the PEO process. Furthermore, the discharge centers are divided into smaller active

sites to avoid the fierce discharges. The extent of spark discharges becomes soft and the diameters of discharge pores in the oxide layer are decreased. Therefore, Glycerol is a wonderful leveler on magnesium alloys during the plasma electrolytic.

Insert Figure 7 Here

The effect of leveler (glycerol) on the PEO process of deposition should be studied in detail. The model for the adsorbed layer of glycerol molecules at the interface is shown in Fig. 8b. Glycerol is a polar liquid with many free and strong polar hydroxyl groups, a high dielectric constant and surface activity at the solid-liquid interface, which gives rise to specific adsorption at the interface between anode and electrolyte in alkali solutions [36], which is in good agreement with MD simulations above. It possible substitutes for the H_2O molecular film formed at the anode-electrolyte interface in the base electrolyte, to some extent, which leads to decrease of the solid-liquid interfacial tension (as shown in Fig. 8d). In addition, as a matter of fact, the anions ionized from Na_2SiO_3 solution predominantly exist in the form of $SiO(OH)_3^-$ and $SiO_2(OH)_2^{2-}$ anions rather than SiO_3^{2-} at pH >13 in the electrolyte [37-39]. Which Silicate ions ($SiO(OH)_3^-$ and $SiO_2(OH)_2^{2-}$) with negative electricity are formed finally through hydrolytic reactions (reaction 8 and reaction 9). Glycerol has three hydroxyl groups that are responsible for its solubility in water and its hygroscopic nature. Silicate ions and $C_3H_8O_3$ molecule have the same structure with OH groups. So, it is possible to conclude that the intermolecular repulsive force between the interface and silicate ions decreases with adsorption of $C_3H_8O_3$ molecules[40]. That is to say, the silicate ions tend to be adsorbed with the $C_3H_8O_3$ molecules due to the fact that they have the similar polarity and affinity for each other. Accordingly, the adsorptive capacity of the negative ions near anode/electrolyte interface is increased because of the mutual attraction. Silicate ions are much denser

at the anode-electrolyte interface under the action of electric field force. Therefore, anode plate is easier to form some kind of chemical interaction with the negative ions and inhibit the area of spark discharge to avoid the partial sintering.

$$SiO_3^{2-} + 2H_2O \rightarrow SiO(OH_3)^- + OH^- \quad (8)$$

$$SiO(OH)_3^- + OH^- \rightarrow SiO_2(OH)_2^{2-} + H_2O \quad (9)$$

Insert Figure 8 Here

Growth of PEO coating could be grown quickly as well as the anode voltage by adding the glycerol, which is in accordance with the result of voltage vs. time. In addition, $C_3H_8O_3$ as an organic molecule could increase the surface resistance when it is adsorbed on the surface of magnesium alloy. This leads to the formation of the dense and uniform discharge centers on the surface of the passivated coating during the PEO process [40]. The active sites on the surface are divided into smaller sizes lead to the decrease of the volume of oxygen bubble. The bigger gas bubble could block the hole by diffusing to prevent the electrolyte pumping into embedded parts. The volume of the oxygen bubble is decreased by adding glycerol, which makes the undersurface could react with the electrolyte during the PEO process (as shown in Fig.9d). Therefore, ceramic coating obtained in electrolyte with proper content of $C_3H_8O_3$ has a smoother surface, less pores and micro-cracks than that obtained in the base electrolytic solution. Thus, the compacter structure of the coating decreases the passages for the eroding anions entering into the coating and thus provides a superior corrosion resistance[40].

3.6 Electrochemical properties of the samples

Insert Figure 9 Here

The potentiodynamic polarization curves of the coatings and bare sample in 3.5 wt.% NaCl solution are shown in Fig. 9, and the associated electrochemical data are listed

in Table 1. All data clearly showed that all of oxide films of the samples treated by PEO in base electrolyte with and without glycerol addition, exhibits better corrosion resistance than that of ZK60 substrate, which indicates that the anti-corrosion property of the magnesium alloy surface has been considerably improved after PEO treatment. Moreover, compared with the coating prepared in basic electrolyte, the ceramic coatings formed in the electrolytic solution containing glycerol have higher corrosion potential and lower current density.

In addition, the corrosion current densities of the PEO coating formed in base electrolyte with 50mL/L and 200mL/L glycerol are 73.04 nA/cm^2 and 44.46 nA/cm^2, respectively. The coating formed in base electrolyte with 100 mL/L glycerol exhibits the most positive corrosion potential (-1.29 V *vs*. Ag/AgCl.) and the lowest corrosion current density (42.98 nA/cm^2). In contrast to the ZK60 substrate, the Ecorr increases 0.28 V while the icorr decreases nearly four orders of magnitude. The bare sample exhibits a corrosion current density of 0.105 mA/cm^2 and an associated corrosion potential of -1.57 V *vs*. Ag/AgCl.

It can be attributed to the fact that the coating formed in the base electrolyte containing 100 mL/L glycerol exhibits the micro-pores with the least micro-cracks. Smaller pores and fewer cracks, as well as the relatively uniform structure of this coating, decrease the passages of the eroding Cl^- anions entering into the coating and thus provides a superior corrosion resistance. Glycerol as an excellent leveler could reduce the surface defects during the plasma electrolytic oxidation. The corrosion resistance of the coating is increased when glycerol is added in low level. However, adding glycerol in excessive amounts may be harmful to corrosion resistant because in that case the adsorbate could act as an eroding anion. On the other hand, with the adding of glycerol, the increasing break voltage accelerates the discharging energy,

leading to the increased product mass by a single pulse and the enlarged pore sizes after the discharged channels are cooled. In addition, the increased voltage induces the heat stress to rupture the coating consequently. The bigger pores and cracks increase the contact area between the corrosive electrolyte and the substrate, but cannot restrict the invasion of Cl^- to protect the magnesium alloy effectively [41].

Insert Table 1 Here

Conclusion

In summary, this study demonstrated corrosion resistance performance of oxide ceramic prepared by plasma electrolytic oxidation method in the base electrolyte with and without glycerol addition.

1. The results of molecular dynamics simulations showed that $C_3H_8O_3$ molecule adsorbed at magnesium surface and could decrease the number of cracks and increase the thickness of ceramic coatings.

2. Glycerol could be used as a new leveler for close-hole and could improve the quality of coating effectively during the plasma electrolytic oxidation process.

3. The lowest corrosion rate is displayed by the coating formed in the electrolyte containing 100 mL/L glycerol, which exhibits the most positive corrosion potential (-1.29 V) and the lowest corrosion current density (42.98 nA/cm^2) by means of electrochemical corrosion test in 3.5 wt.% NaCl solution.

Acknowledgement

This work was financially supported by the National Natural Science Foundation of China (No.11374080).

References

1. A. Bussiba, A. B. Artzy, A. Shtechman, S. Ifergan and M.Kupiec, *Mat. Sci. Eng A-Struct.* 2001, **302**, 56-62.

2. X. H. Wu, P. B. Su, Z. H. Jiang and S. Meng, *ACS Appl. Mater. Inter.* 2010, **2,** 808-812.
3. M. I. Jamesh, G. Wu, Y. Zhao, D. R. McKenzie, M. M. Bilek and P. K. Chu, *Corros. Sci.* 2014, **82**, 7-26.
4. G. L. Makar and J. Kruger, *Int. Mater. Rev*. 1993, **38**, 138-153.
5. X. B. Chen, N. Birbilis and T. B. Abbott, *Corros. Sci.* 2012, **55**, 226-232.
6. G. Song and A. Atrens, *Adv. Eng. Mater.* 2007, **9**, 177-183.
7. J. Liang, P.B. Srinivasan, C. Blawert, M. Störmer and W. Dietzel, *Electrochim. Acta*. 2009, **54**, 3842-3850.
8. A. Alabbasi, K. M. Bobby, R. Walter, M. Störmer and C. Blawert, *Mater. Lett.* 2013, **106**, 18-21.
9. Y. Mori, A. Koshi, J. Liao, H. Asoh and S. Ono, *Corros. Sci.*, 2014, **88**, 254-262.
10. J. Liang, B. Guo, J. Tian, H. Liu, J. Zhou, W. Liu and T. Xu, *Surf. Coat. Tech.*, 2005, **199**,121-126.
11. O. Khaselev, D. Weiss and J. Yahalom, *Corros. Sci.,* 2001, **43**, 1295-1307.
12. H. X. Li, V. S. Rudnev, X. H. Zheng, T. P. Yarovayab and R. G. Song, *J. Alloys Compd.,* 2008, **462**, 99-102.
13. M. Faghihi-Sani, A. Arbabi and A. Mehdinezhad-Roshan, *Ceram. Int.*, 2013, **39**, 1793-1798.
14. H. L. Wu, Y. L. Cheng, L. L. Li, Z. Chen, H. Wang and Z. Zhang, *Appl. Surf. Sci*., 2007, **253**, 9387-9394.
15. H. F. Guo and M. Z. An, *Thin Solid Films*, 2006, **500**, 186-189.
16. R. F. Zhang, S. F. Zhang and S.W. Duo, *Appl. Surf. Sci.*, 2009, **255**, 7893-7897.

17. M. Pagliaro, R. Ciriminna, H. Kimura, M. Rossi and P. C. Della, *Angew. Chem. Int. Edit.*, 2007, **46**, 4434-4440.

18. Y. L. Gu and F. Jerome, *Green. Chem.*, 2010, **12**, 1127-1138.

19. I. A. Carlos, M. A. Malaquias, M. M. Oizumi and T. T. Matsuo, *J. Power. Sources*, 2001, **92**, 56-64.

20. M. G. Hosseini, S. A. S. Sajjadi and M. M. Momeni, *Surf. Eng.*, 2007, **23**, 419-424.

21. E. M. De Oliveira and I. A. Carlos, *J. Appl. Electrochem.*, 2008, **38**, 1203-1210.

22. E. M. Oliveira, G. A. Finazzi and I. A. Carlos, *Surf. Coat. Tech.*, 2006, **200**, 5978-5985.

23. A. G. Morachevskii, A. I. Demidov, Z. I. Vaisgant and M. S. Kogan, *Russ. J. Appl. Chem.*, 1996, **69**, 412-414.

24. E. M. De Oliveira, W. Rubin, I. A. Carlos, J. Appl. Electrochem. 2009, **39**, 1313-1321.

25. A. L. Yerokhin, X. Nie, A. Leyland, A. Matthews and S. J. Dowey, *Surf. Coat. Tech.*, 1999, **122**, 73-93.

26. S. Xia, M. Qiu, L. Yu, F. Liu and H. Zhao, *Corros. Sci.*, 2008, **50**, 2021-2029.

27. C. Wang, M. Z. An, P. Yang and J. Zhang, *Electrochem. Commun.*, 2012, **18**, 104-107.

28. L. Zhao, C. Cui, Q. Wang and S. Bu, *Corros. Sci.*, 2010, **52**, 2228-2234.

29. A. K. Sharma, R. U. Rani and S. M. Mayanna, *Thermochim. Acta*, 2001, **376**, 67-75.

30. Y. Zhang, C. Yan, F. Wang and W. Li, *Corros. Sci.*, 2005, **47**, 2816-2831.

31. R. F. Zhang and S. F. Zhang, *Corros. Sci.*, 2009, **51**, 2820-2825.

32. J. M. Albella, I. Montero and J. M. Martinez-Duart, *Electrochim. Acta*., 1987, **32**, 255-258.

33. A. K.Vijh, *Corros. Sci.*, 1971, **11**, 411-417.

34. X. Zhou, G. E. Thompson, P. Skeldon, G. C. Wood, K. Shimizu and H. Habazaki, *Corros. Sci.*, 1999, **41**, 1599-1613.

35. G. Raffaini and F. Ganazzoli, *J. Mater. Sci.*, 2007, **18**, 309-316

36. L. M. Feng, Y. Wang and F. H. Sun, Electroplating Technology and Equipments, Chemical Industry Press, Beijing, in Chinese. 2005.

37. Z. Shen and G. T. Wang, Colloid and Surface Chemistry, Chemical Industry Press, Beijing, in Chinese,1997.

38. X. Yang, P. Roonasi and A. Holmgren, *J. colloid. Interf. Sci.*, 2008, **328**, 41-47.

39. I. Halasz, M. Agarwal, R. Li, and N. Miller, *Catal. Lett.*, 2007, **117**, 34-42.

40. D. Wu, X. Liu, K. Lu, Y. Zhang and H. Wang, *Appl. Surf. Sci.* 2009, **255**, 7115-20.

41. Z. Z. Qiu, R. Wang, Y. S. Zhang, Y. F Qu, and X. H. Wu, 2015, **24**, 1483–1491

Figure captions

Fig.1 Voltage-time curve of the sample during PEO process.

Fig.2. Cross-sectional morphologies of the PEO coating obtained under containing with different concentrations of glycerol, (a) 0 mL/L, (b) 50 mL/L, (c) 100 mL/L, (d) 200 mL/L.

Fig.3 the corresponding EDS and element-mapping data, (a) Typical SEM image, (b) EDS, (c–f) chemical element mapping data.

Fig.4 XRD patterns of PEO ceramic coatings processed for 6 min in base electrolyte. (a) with 200mL/L glycerol addition, (b) with 100mL/L glycerol addition, (c) with 50 mL/L glycerol addition, (d) the base electrolyte

Fig.5 the surface morphologies of the PEO coating obtained under containing different concentrations of glycerol, (a) 0 mL/L, (b) 50 mL/L, (c) 100 mL/L, (d) 200 mL/L.

Fig.6. the photograph of embedded parts of magnesium alloy after PEO process in the glycerol electrolyte, (a) 0 mL, (b) 100mL.

Fig.7 (a) Initial configuration of the simulation box; (b) Final equilibrium configuration. ($C_3H_8O_3$ visualized by balls and sticks, water molecule visualized by lines)

Fig.8 Schematic illustration of the SiO_3^{2-} distribution at anode/electrolyte interface in two different electrolytes at the primary stages of the PEO treatment. (a) in basic electrolyte, (b) in the basic electrolyte with glycerol, (c) discharge mechanism of the basic electrolyte, (d) discharge mechanism of the basic electrolyte containing glycerol.

Fig.9 Potentiodynamic polarization curves of the coatings formed in different conditions and Zk60 alloy substrate in 3.5 wt.% NaCl solution.

Table caption

Table 1 Electrochemical data from the polarization tests of the PEO coatings prepared in the base electrolyte with and without glycerol on ZK60 alloy in 3.5 wt.% NaCl solution.

Sample	E_{corr} (V vs. Ag/AgCl)	i_{corr} (nA/cm^2)	β_c (mV/dec)	β_a (mV/dec)
0 mL	-1.36	89.15	-639.53	159.51
50 mL	-1.32	73.04	-249.05	313.74
100 mL	-1.29	42.98	-352.81	125.31
200 mL	-1.27	44.46	-104.76	355.96
Substrate	-1.57	105000	-198.95	34.98

Fig.1 Voltage-time curve of the sample during PEO process.

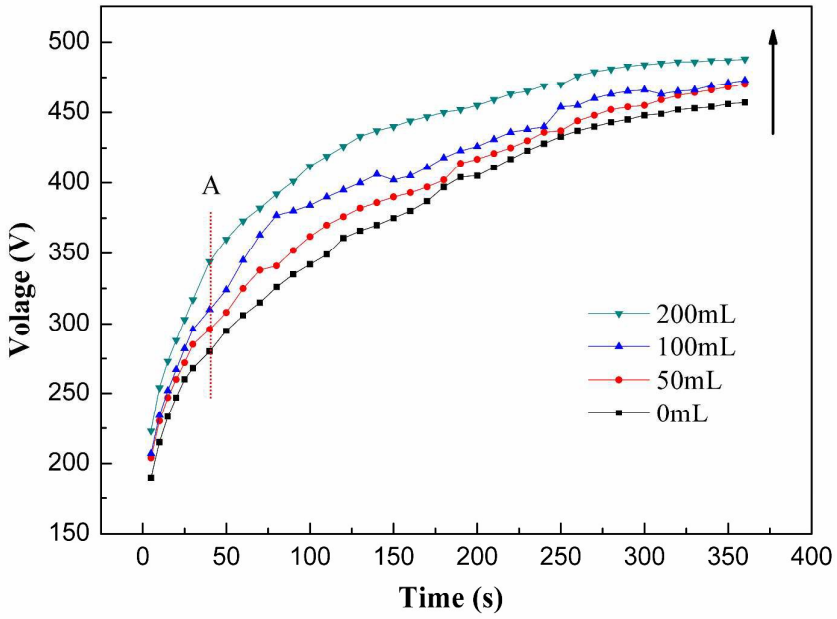

Fig.2. Cross-sectional morphologies of the PEO coating obtained under containing with different concentrations of glycerol, (a) 0 mL/L, (b) 50 mL/L, (c) 100 mL/L, (d) 200 mL/L.

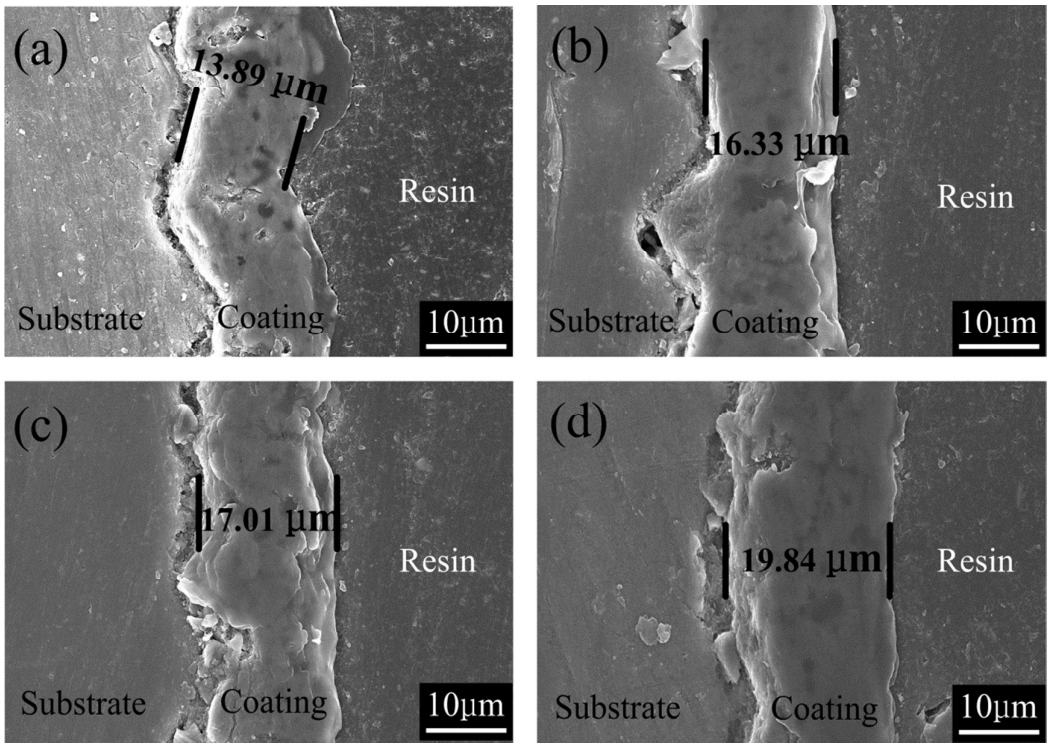

Fig.3 the corresponding EDS and element-mapping data, (a) Typical SEM image, (b) EDS, (c–f) chemical element mapping data.

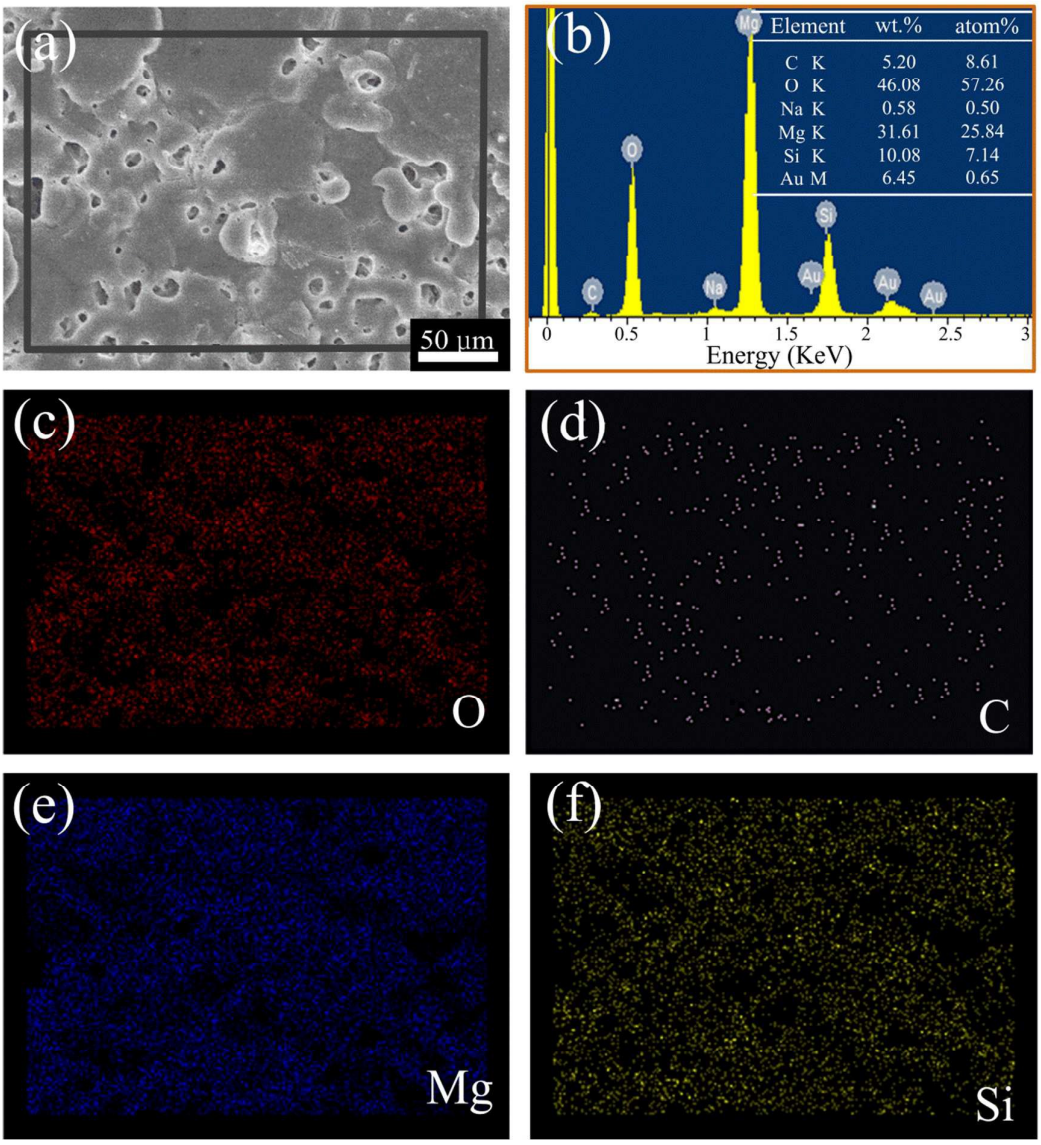

Fig.4 XRD patterns of PEO ceramic coatings processed for 6 min in base electrolyte. (a) with 200mL/L glycerol addition, (b) with 100mL/L glycerol addition, (c) with 50 mL/L glycerol addition, (d) the base electrolyte.

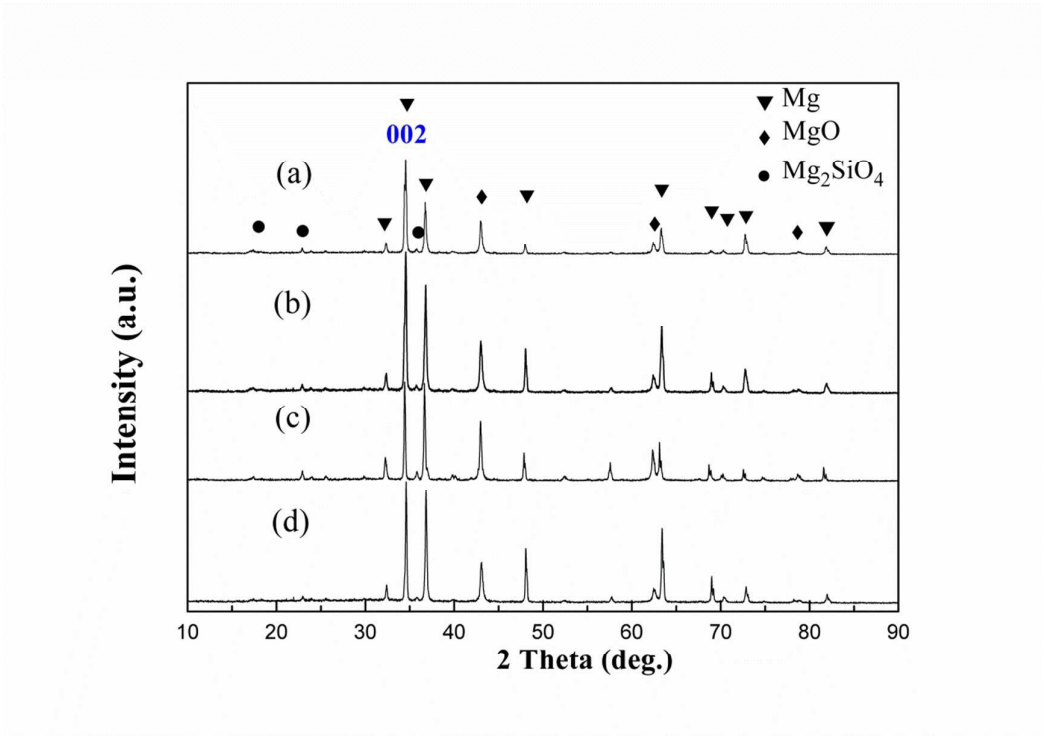

Fig.5 the surface morphologies of the PEO coating obtained under containing different concentrations of glycerol, (a) 0 mL/L, (b) 50 mL/L, (c) 100 mL/L, (d) 200 mL/L.

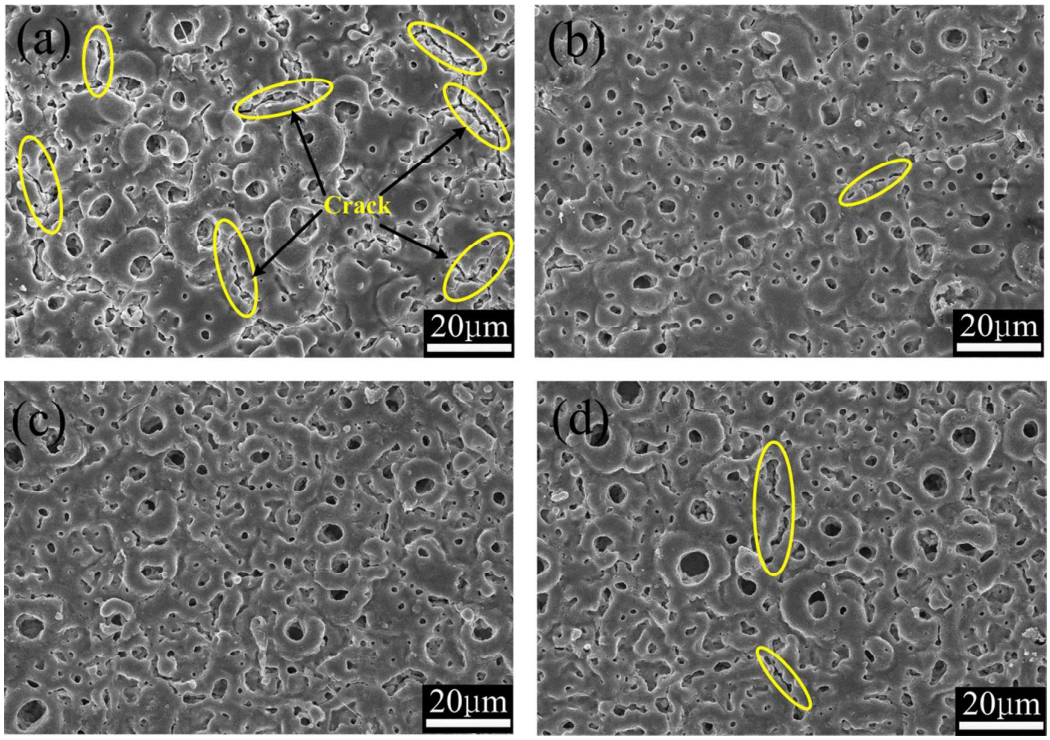

Fig.6. the photograph of embedded parts of magnesium alloy after PEO process in the glycerol electrolyte, (a) 0 mL, (b) 100mL.

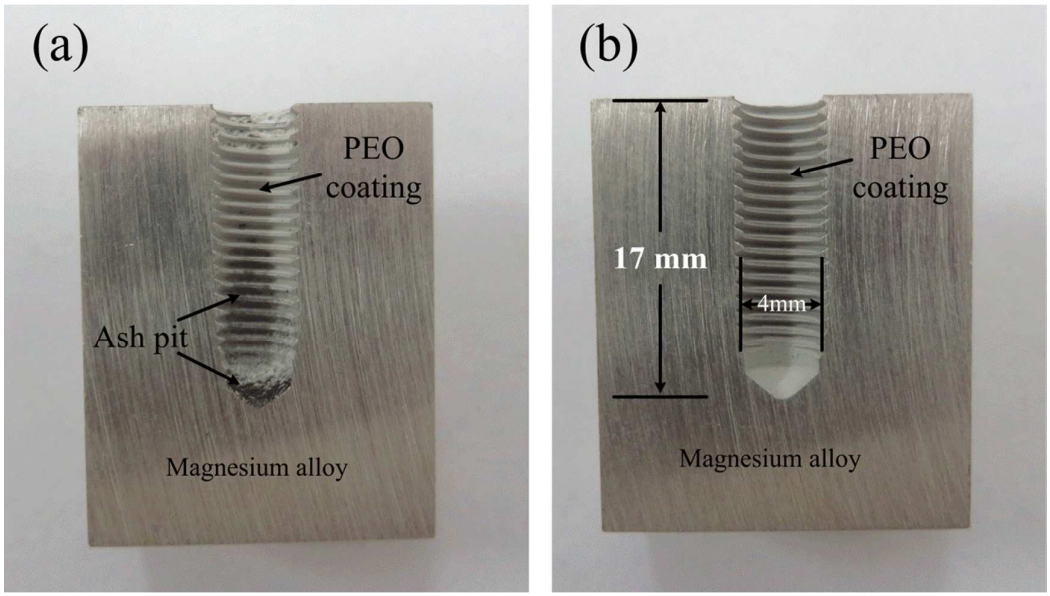

Fig.7 (a) Initial configuration of the simulation box; (b) Final equilibrium configuration. ($C_3H_8O_3$ visualized by balls and sticks, water molecule visualized by lines)

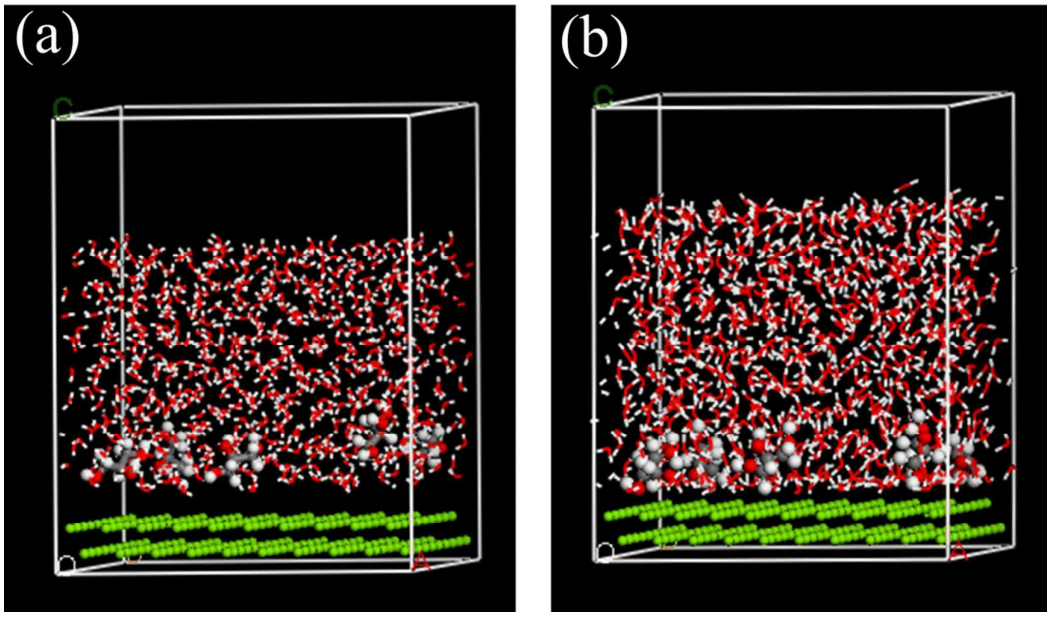

Fig.8 Schematic illustration of the SiO_3^{2-} distribution at anode/electrolyte interface in two different electrolytes at the primary stages of the PEO treatment. (a) In base electrolyte, (b) In the base electrolyte with glycerol, (c) discharge mechanism of base electrolyte, (d) discharge mechanism of base electrolyte containing glycerol.

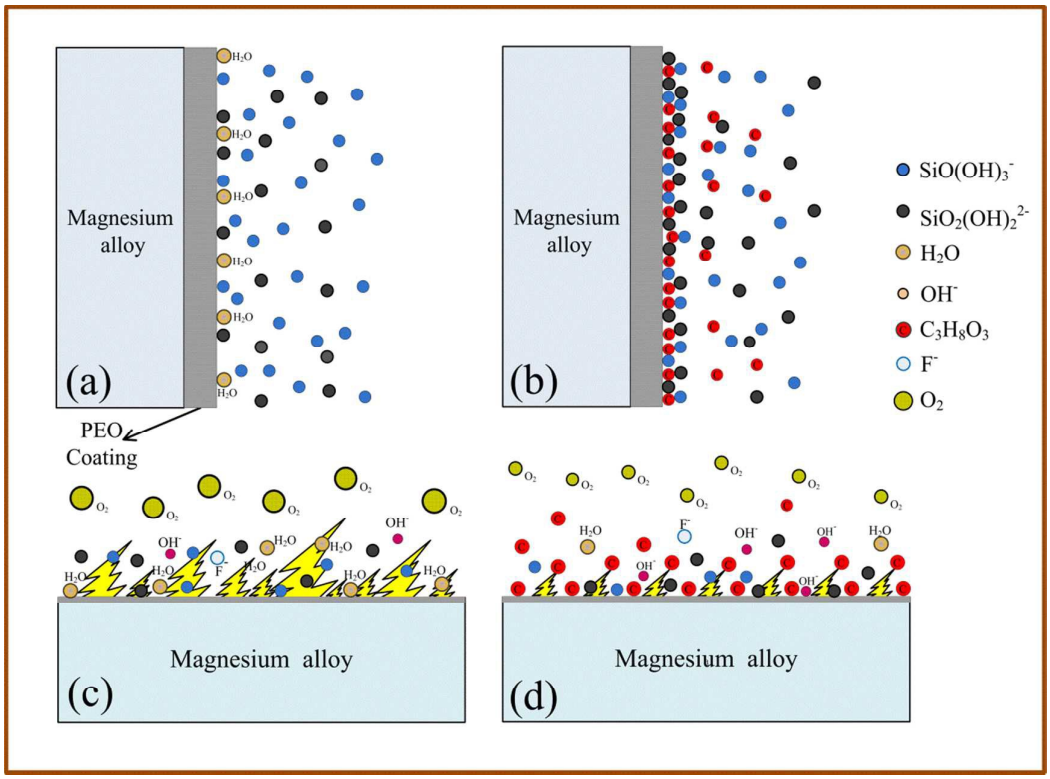

Fig.9 Potentiodynamic polarization curves of the coatings formed in different conditions and Zk60 alloy substrate in 3.5 wt.% NaCl solution.